ACS SENSORS

pubs.acs.org/acssensors

Article

3D-Printed Flexible Microfluidic Health Monitor for *In Situ* Sweat Analysis and Biomarker Detection

Chuchu Chen, Yonghao Fu, Sonja S. Sparks, Zhaoyuan Lyu, Arijit Pradhan, Shichao Ding, Narasimha Boddeti, Yun Liu, Yuehe Lin, Dan Du,* and Kaiyan Qiu*

Cite This: *ACS Sens.* 2024, 9, 3212−3223

Read Online

ACCESS | Metrics & More | Article Recommendations | Supporting Information

ABSTRACT: Wearable sweat biosensors have shown great progress in noninvasive, *in situ*, and continuous health monitoring to demonstrate individuals' physiological states. Advances in novel nanomaterials and fabrication methods promise to usher in a new era of wearable biosensors. Here, we introduce a three-dimensional (3D)-printed flexible wearable health monitor fabricated through a unique one-step continuous manufacturing process with self-supporting microfluidic channels and novel single-atom catalyst-based bioassays for measuring the sweat rate and concentration of three biomarkers. Direct ink writing is adapted to print the microfluidic device with self-supporting structures to harvest human sweat, which eliminates the need for removing sacrificial supporting materials and addresses the contamination and sweat evaporation issues associated with traditional sampling methods. Additionally, the pick-and-place strategy is employed during the printing process to accurately integrate the bioassays, improving manufacturing efficiency. A single-atom catalyst is developed and utilized in colorimetric bioassays to improve sensitivity and accuracy. A feasibility study on human skin successfully demonstrates the functionality and reliability of our health monitor, generating reliable and quantitative *in situ* results of sweat rate, glucose, lactate, and uric acid concentrations during physical exercise.

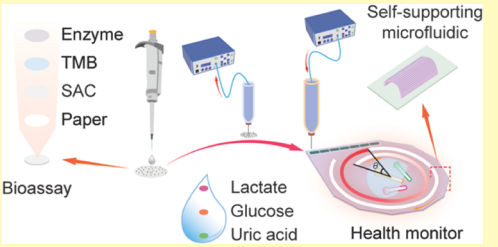

KEYWORDS: *wearable health monitor, self-supporting microfluidics, sweat analysis, biomarker detection, single-atom catalyst*

Wearable biosensors hold great potential for noninvasive and continuous tracking of health conditions and disease diagnosis,[1−3] providing individuals with a comprehensive insight into their dynamic physiological status.[4−7] Human sweat is a noninvasive biofluid and can be readily sampled from the high density of sweat glands (over 100 glands/cm^2)[8] in the human body. Sweat consists of abundant biomarkers, such as metabolites (glucose,[9,10] uric acid,[11] lactate,[12] etc.) and electrolytes (Na^+, Cl^-, K^+, Ca^{2+}, Zn^{2+}, and Cu^{2+}).[13−15] The levels of biomarkers indicate the risks for developing potential diseases.[16] Glucose in sweat has been reported to accurately reflect blood glucose.[17] Measuring the glucose levels in sweat is beneficial for diabetes management. Uric acid is the end product of purine metabolism. Uric acid levels in sweat indicate the risks of developing gout, kidney disease, or other cardiovascular diseases.[18] Lactate is a byproduct of anaerobic metabolism, and its concentration in sweat can reflect the exercise intensity and physiological conditions.[19] Therefore, real-time monitoring for the concentration of target biomarkers is beneficial for initial noninvasive assessment of metabolic and physiological statuses, enabling personalized healthcare interventions and early detection of health issues.[20] Excessive sweat rate implies the potential of developing dehydration or hyperhidrosis.[21] Monitoring sweat rate is essential for enhancing athletic performance,[22,23] ensuring physical health, and aiding in disease management.[24]

Numerous wearable sweat sensors have arisen and demonstrated a wealth of sensing scenarios to monitor various molecular-level physiological parameters.[25,26] Up to now, colorimetric biosensors are often integrated with soft microfluidic systems for *in situ* sweat collection and analysis.[10,27−30] However, the majority of existing wearable microfluidic sweat biosensors are fabricated by soft lithography techniques, which are complex and demand specialized equipment and expertise.[31] The low concentrations of biomarkers in sweat pose significant challenges for the advancement of wearable biosensors.[32] Therefore, alternative fabrication techniques, enhanced sensitivity, and incorporation methods are still urgently required for developing advanced wearable microfluidic devices.

Conventional sweat sampling methods include patches,[33] whole body washdown,[34] and Macroducts,[35] involving impedance from skin contamination, sweat rate effects, and sweat evaporation.[36] These collection techniques require professional handling for precision analysis after sampling

Received: March 5, 2024
Revised: May 4, 2024
Accepted: May 21, 2024
Published: May 31, 2024

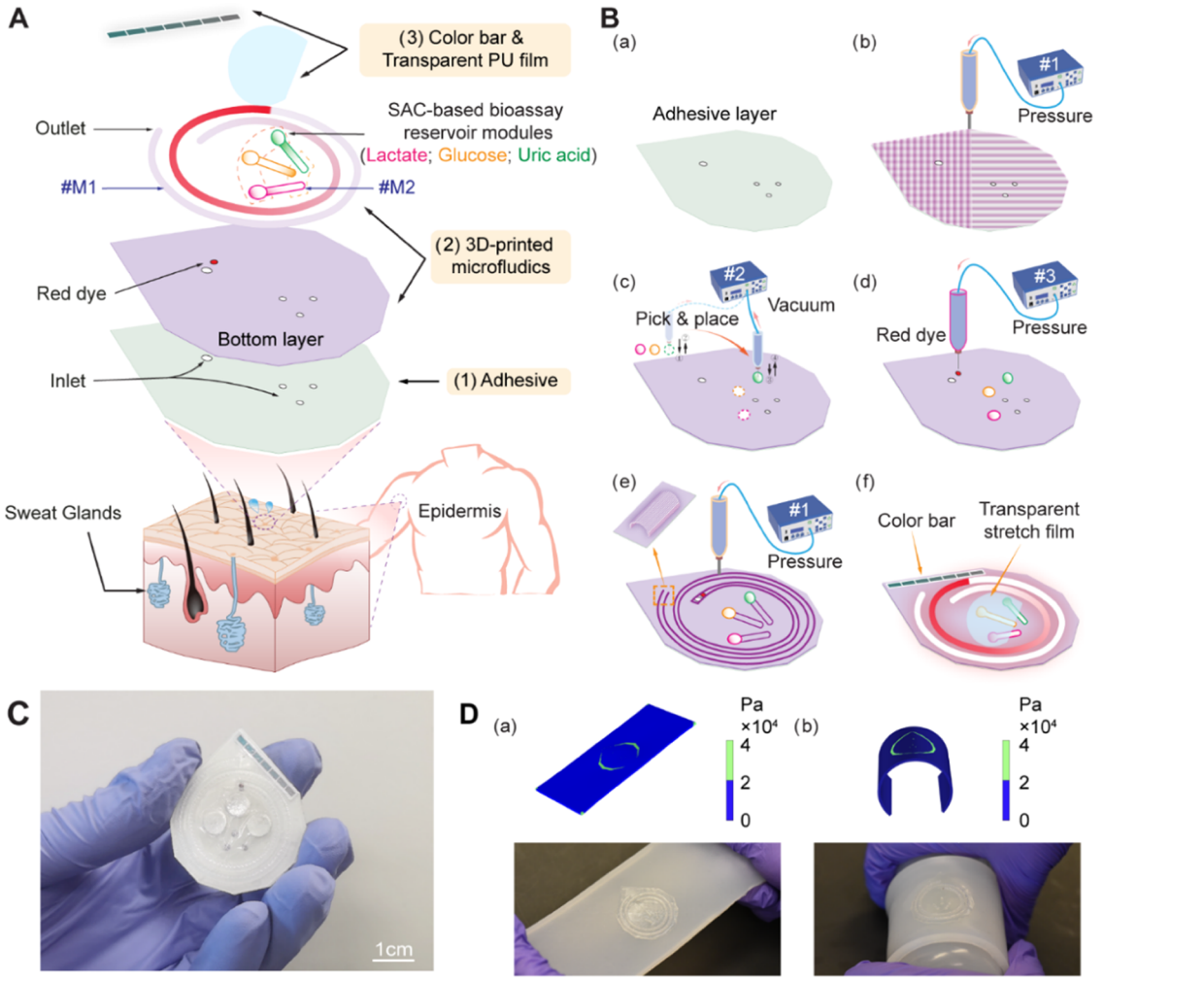

Figure 1. Design and fabrication of the 3D-printed flexible microfluidic health monitor. (A) Schematic of the wearable flexible health monitor; (B) 3D-printing process of the wearable health monitor with microfluidic channel and SACs-based bioassays: (a) Adhesive layer with predefined inlet holes, (b) DIW for the bottom layer, (c) PNP process for SACs-based colorimetric bioassays via vacuum mode, (d) Red dye was dripped close to the inlet of the microfluidic channel, (e) DIW for self-supporting microfluidic channel, (f) Transparent/stretchable film was covered, and the color reference bar was added; (C) optical image of a fabricated health monitor, scale bar, 1 cm; and (D) FEA simulation results (stress) and their corresponding optical images of the health monitor on Ecoflex 00−30 skin during (a) stretching (elongation of 12 mm) and (b) bending (radius of curvature 30 mm).

and cannot provide instant feedback, thus limiting their applications.[37] Advances in materials and fabrication methods bring out the possibilities of epidermal microfluidic systems for continuous monitoring and real-time analysis.[27,31,38] Microfluidics provides benefits to microliter-scale chemical and biological research because of the advantages of small sample volumes and well-controlled microenvironments.[39]

Critical physicochemical requirements for substrate materials in wearable sensors include flexibility,[40] stretchability,[15] dimensional stability,[41] and water resistance.[42] Polymers are the most popular functional materials for wearable sensors due to a wealth of physical/chemical modification strategies and their diverse traditional fabrication methods[43] or novel manufacturing approaches, such as three-dimensional (3D) printing.[44] With the advantages of low manufacturing cost, easy availability, and customized options,[45] 3D printing has recently emerged as an alternative fabrication method for microfluidics.[46] Most 3D-printed microfluidic devices have channel sizes from hundreds of microns to a few millimeters.[47] The 3D-printing process usually requires sacrificial supporting materials to fill the voids. However, supporting materials are typically difficult to remove manually and block channel sections with sharp bends and complicated inner designs, limiting the use of 3D printing to fabricate structures for microfluidic devices.[48]

Due to the low concentration level of the sweat components, the sensing module of wearable sweat sensors is required to demonstrate high sensitivity and excellent selectivity for the quantitative detection of sweat biomarkers.[1,2,40] Enzyme-based colorimetric methods have been used in a variety of biosensors over the past decades.[49−52] Nanozymes are nanomaterials that mimic natural enzyme properties and possess excellent stability, low cost, easy production, and high catalytic activity, which overcome the drawbacks of natural enzymes.[53,54] Among the nanozymes, single-atom catalysts (SACs) with atomically dispersed metal atoms as active sites on their supports have higher catalytic activity and selectivity than traditional nanozymes, endowing the biosensors with higher sensitivity and realizing the sensitive detection of trace biomolecules.[55,56] Iron−nitrogen−carbon single-atom catalysts

https://doi.org/10.1021/acssensors.4c00528
ACS Sens. 2024, 9, 3212−3223

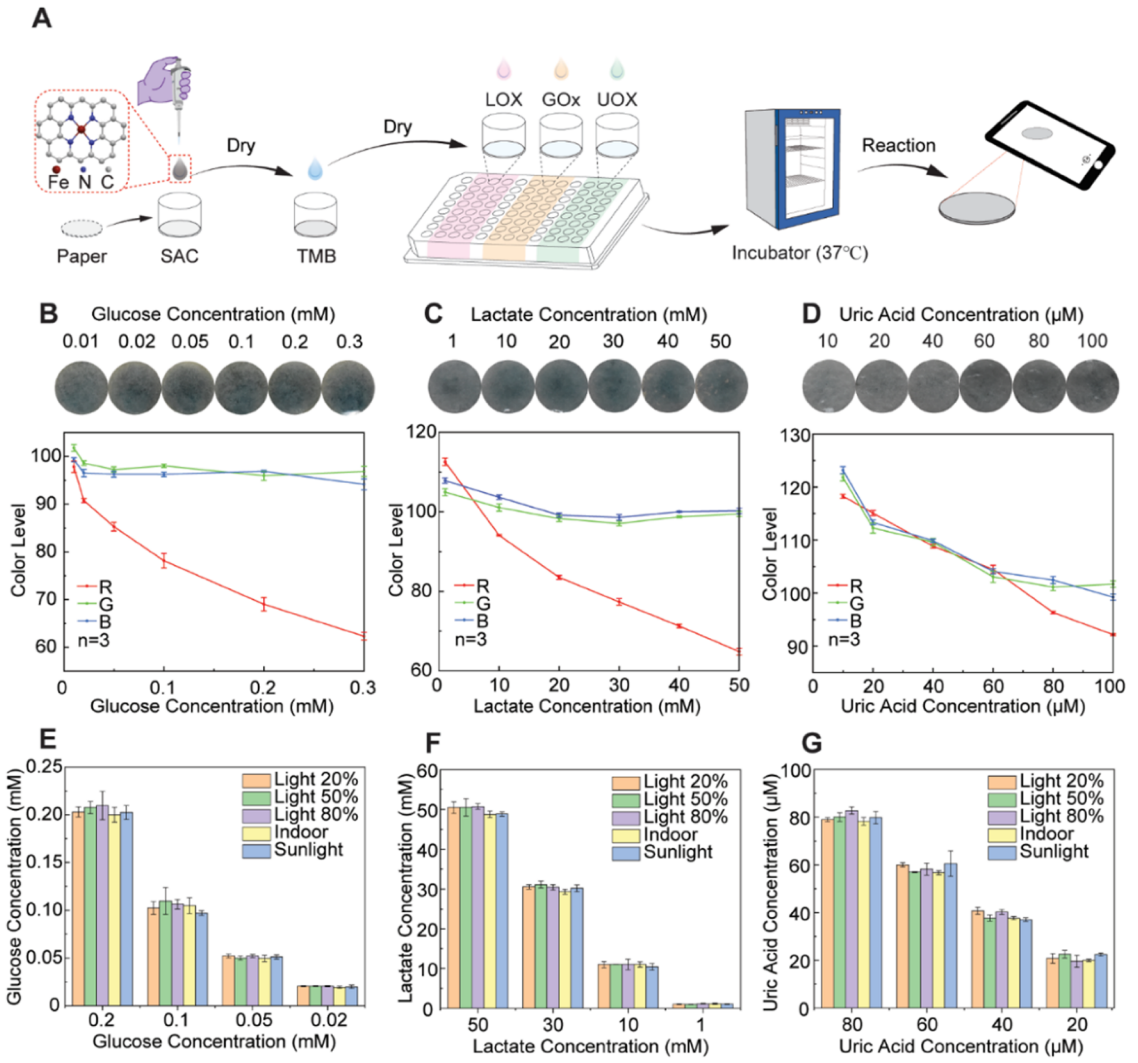

Figure 2. SACs-based bioassay preparation and quantitative colorimetric. (A) Fabrication of bioassays. (B–D) Color change of bioassays and *R*, *G*, and *B* values with different (B) glucose, (C) lactate, and (D) uric acid concentrations. (E–G) Comparison of (E) glucose, (F) lactate, and (G) uric acid concentrations measured under different light conditions using color reference and standard concentration. Different light conditions (light 20%, light 50%, and light 80%) were obtained by controlling adjustable light bulbs. The higher the percentage value, the brighter the light. Indoor: the images were taken in a room. Sunlight: the images were taken in the sun.

(Fe–N–C SACs) that mimic the natural metalloenzyme structure have well-defined metal atom bond configurations, high level of molecular selectivity, and are easy to fabricate, enabling single-molecule detections with practical-use feasibilities.[57] The Fe–N–C SACs that were synthesized by previous work show excellent peroxidase-like activity.[58,59] It has been proven that Fe–N–C SACs can be used in a series of bioassays for ultrasensitive detection of H_2O_2, glucose, and amide acid.[60]

Herein, we present a disposable and flexible wearable health monitor featuring self-supporting microfluidic channels and novel SACs-based bioassays, which were fabricated in one continuous step by 3D printing with direct ink writing (DIW) and using a pick-and-place (PNP) strategy. These self-supporting structures in the microfluidic channels of our health monitor eliminate the need for sacrificial supporting materials during manufacturing. These channels enable accurate *in situ* measurement of sweat rate, addressing concerns related to skin contamination and evaporation during sweat sampling. The SACs-based bioassays in the health monitor were utilized for enzymatic reactions and colorimetric sensing to detect three biomarkers in sweat with linear ranges of 0.01–0.3 mM for glucose, 1–50 mM for lactate, and 10–100 μM for uric acid, respectively, which are in good agreement with the clinical concentration range of healthy people. The PNP strategy facilitated the precise integration of SAC-based bioassays into the health monitor, streamlining the process without the need for additional manual operations. In combination, our proof-of-concept work overcomes the inherent limitations in sensing sensitivity and simplifies fabrication complexity for *in situ* sweat monitoring using microfluidic channels while ensuring excellent wearability and comfort. Furthermore, this integrated system demonstrates the potential for expansion and customization to monitor multiple sweat biomarkers, providing valuable physiological insights for health monitoring.

RESULTS AND DISCUSSION

The wearable flexible health monitor introduced here is fabricated by the DIW method and integrated by PNP strategy

https://doi.org/10.1021/acssensors.4c00528
ACS Sens. 2024, 9, 3212–3223

for *in situ* sweat analysis and biomarker detection. Figure 1A illustrates the design of a 3D-printed flexible wearable health monitor. The system consists of three major components from bottom to top: (1) a medical-grade subjacent skin adhesive layer (~0.06 mm, 3M 1524 Medical Transfer Adhesive) with four predefined inlets (three inlets for connecting with the bioassay reservoir modules, one inlet for connecting with the spiral microfluidic channel) for skin-interfaced adhesion to the human skin, (2) a 3D-printed microfluidic component with a bottom layer (thickness, ~ 0.45 mm), food-grade red dye, and microfluidic channel (#M1 for measuring sweat rate and #M2 for connecting with bioassay reservoir modules, wall thickness, ~0.45 mm) for sweat collection and measurement, and (3) three SACs-based bioassays covered by a transparent and flexible polyurethane (PU) film and a color reference bar for colorimetric and quantitative detection of biomarkers concentrations (glucose, uric acid, and lactate, respectively). The one-step fabrication process involving three nozzles and three pneumatic dispensers for 3D printing is depicted in Figure 1B and Movie S1: (a) the adhesive layer with defined inlets was placed at a designated position of the 3D-printing platform; (b) the bottom layer was printed by extrusion-based DIW method with pneumatic pressure; (c) three paper-based bioassays were integrated one by one via an empty nozzle using an automatic PNP strategy with vacuum setting;[61,62] (d) food-grade red dye was dripped with air pressure to the 3D-printed bottom layer; (e) the self-supporting microfluidic channels were printed layer-by-layer; (f) a transparent stretch PU film was used to cover the bioassays to avoid the oxidation by air, and a color reference bar was added for color reference and white balance to establish the true color of white.

The microfluidic component was fully 3D-printed with biocompatible and hydrophobic silicone-based polymeric inks. The capacity of the spiral microfluidic channel is about 78 μL with a circular sweat collection zone (1 mm in diameter). Theoretically, this spiral microfluidic channel is capable of collecting sweat for more than 30 min, depending on the exercise intensities. The driving force comes from the natural pressure (3−70 kPa, average: 40 kPa[63]) during the excretion process of sweat glands.[6,64] Water-soluble food-grade red dye was dripped from the inlet for favorable observation of the filling front (the front edge of the color change). Microfluidic channels for colorimetric sensing hold smaller volumes (~5 μL for each) and collection areas (1 mm in diameter). The medical polyester fiber-reinforced tackified acrylic adhesive film yielded a stable adhesion between the self-supporting microfluidic component and human skin. The low modulus and high elasticity of our silicone-based inks for microfluidic components and stretchable adhesive rendered the whole health monitor (thickness: 1.56 mm) with excellent flexibility and wearability (Figure 1C).

To demonstrate that the stresses on the skin remained below the somatosensory limit for verifying the comfortable wearability of our health monitor, we conducted finite element analysis (FEA) using a CAD model comprising a phantom skin (Ecoflex 00−30 by casting, 140 mm × 65 mm × 2.5 mm), an adhesive layer, and the microfluidic device in COMSOL Multiphysics 6.2. The mesh used for FEA is shown in Figure S1A. Two numerical experiments were performed: one for stretching and one for bending. In the stretching experiment, the skin was elongated by 12 mm, and the maximum value of the von-Mises stress on the skin was well within the somatosensory limit of 20 kPa[30,65,66] as shown in Figure 1D(a). For the bending experiment, the model was wrapped around a physical cylinder of radius 30 mm, resulting in a maximum von-Mises stress on the skin still below the somatosensory limit, as depicted in Figure 1D(b). In both models, the higher values observed near locations having sharp changes in the geometric features such as corners and the interface between the skin and adhesive layer may be attributed as a numerical artifact. The corresponding resultant principal strain on the skin is depicted in Figure S1B,C and Supporting Information Text.

The colorimetric sensing strategy enables a simple and quantitative analysis of the concentration of biomarkers in the sweat. Figure 2A illustrates the preparation process of Fe−N−C SACs-based bioassays to detect glucose, lactate, and uric acid in human sweat by colorimetric method. The Fe−N−C SACs, 3,3′,5,5′-tetramethylbenzidine (TMB), and three different oxidases were dropped onto the filter paper, and then the filter papers were dried in a 37 °C incubator for 5 min to obtain bioassays used for the detection of biomarkers. The detailed synthesis process of Fe−N−C SACs is described in the Supporting Information and illustrated in Figure S2. Briefly, $Zn(NO_3)_2$ and 2-methylimidazole reacted with each other to form zeolitic imidazolate framework-8 (ZIF-8), which is a class of metal-organic frameworks (MOFs). The ZIF-8 absorbed Fe^{3+} to form $Fe(NO_3)_3$-doped ZIF-8 as the precursor (ZIF-8@$Fe(NO)_3$). After pyrolysis, the Fe−N−C SACs were obtained. The transmission electron microscopy (TEM) and high-angle annular dark-field scanning transmission electron microscopy (HAADF-STEM) images show the characterization results of the Fe−N−C SACs (Figure S3). Fe−N−C SACs of similar shape and size (rhombic dodecahedral) were observed in the TEM images of the Fe−N−C SACs solution with a concentration of 1 mg/mL (Figure S3A). In Figure S3B, the Fe−N−C SACs solution with a concentration of 0.1 mg/mL avoided the overlap of Fe−N−C SACs and allowed the rhombic dodecahedral structure of Fe−N−C SACs to be more clearly displayed in the TEM image. The HAADF-STEM image shows bright spots (marked by circles), which are attributed to Zn and Fe atoms. The presence of these dispersed single metal atoms confirms the single-atom feature of Fe−N−C SACs. Our previous study demonstrates that the Michaelis constant K_m of Fe−N−C SACs for H_2O_2 is comparable to that of natural horseradish peroxidase (HRP).[67] However, the K_m for TMB is about 100 times smaller than that of HRP, which means a significantly greater affinity of Fe−N−C SACs for TMB compared to HRP. These bioassays were placed into the health monitor attached to the skin to test the biomarkers in sweat. Figure S4 shows the reaction process on bioassays. Glucose, lactate, and uric acid produce H_2O_2 with the catalysis of glucose oxidase (GOx), lactate oxidase (LOX), and urate oxidase (UOX) on glucose, lactate, and uric acid bioassays, respectively. Subsequently, due to the superior peroxidase-like activity of SACs, the reaction of H_2O_2 and TMB could induce the color change of TMB from colorless to blue rapidly. The bioassay images after the color change are shown in Figure 2B−D. As the concentration of biomarkers increases, the color change of the bioassays becomes more obvious. After color calibration and white balance calibration, reliable red, green, and blue (*R*, *G*, and *B*) values of color were obtained, including glucose, lactate, and uric acid detections. In Figure 2B, with the increase of glucose concentration from 0.01 to 0.3 mM, the *R*, *G*, and *B* values decreased from 97.85, 101.80, and 99.30 to 62.32, 96.84, and 94.17, respectively. In Figure 2C, with the

https://doi.org/10.1021/acssensors.4c00528
ACS Sens. 2024, 9, 3212−3223

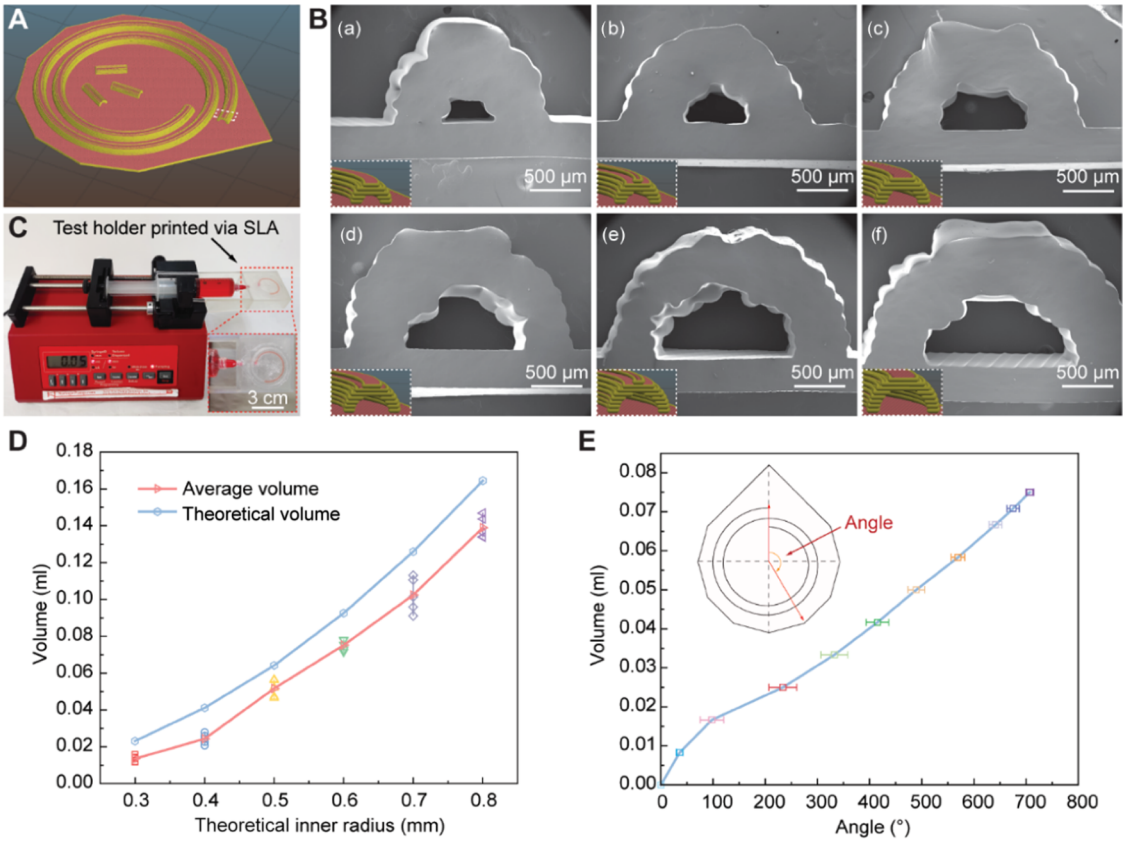

Figure 3. Design and analysis of the self-supporting microfluidic channel in the health monitors. (A) 3D models of the designed structure via Slic3R; (B) cross-sectional SEM images of the 3D-printed self-supporting microfluidic channels with the designed inner radii: (a) 0.3 mm, (b) 0.4 mm, (c) 0.5 mm, (d) 0.6 mm, (e) 0.7 mm, and (f) 0.8 mm; (C) experimental setup of the channel volume testing system at a rate of 0.1 mL/min; (D) experimentally determined microfluidic volumes; and (E) correlation of the filling front angle and corresponding volume from the inlet to the filling front point.

increase of lactate concentration from 1 to 50 mM, the *R*, *G*, and *B* values decreased from 112.56, 104.96, and 107.86 to 64.85, 99.48, and 100.25, respectively. In Figure 2D, with the increase of uric acid concentration from 10 to 100 μM, the *R*, *G*, and *B* values decreased from 118.26, 121.81, and 123.18 to 92.16, 101.68, and 99.23, respectively. The results of fitting linear curves between the biomarker concentration and the values of *R*, *G*, and *B* show that the *R* value has the strongest correlation with biomarker concentration, while the variations in *G* and *B* values across biomarker concentrations are minimal. Therefore, using the standard curve of the *R* value is more accurate for determining the biomarker concentrations. The curved lines between the *R* value of images and concentrations of biomarkers are shown in Figure S5. The *R*-squares of the three fitted curves all exceeded 0.95, indicating a high linear correlation between concentrations of biomarkers and *R* values. The limit of detection (LOD) was determined by using the following equation: LOD = 3 × *S*/*N*, where *S* represents the standard deviation of the signal derived from a blank solution, and *N* is the slope of the calibration curve.[68] The LOD of glucose, lactate, and uric acid were 0.038, 6.76, and 6.98 μM, respectively. In the Supporting Information, Table S1 shows the comparison of the linear detection range and LOD of the device in this study with other wearable sensors. Consequently, the *R* values of bioassays were determined to obtain the concentration of biomarkers, and the detection ranges of glucose, lactate, and uric acid were 0.01−0.3 mM, 1−50 mM, and 10−100 μM (Figure S5). Meanwhile, the concentration ranges of glucose, lactate, and uric acid in human sweat have been reported at 0.01−0.2 mM, 5−40 mM, and about 10−80 μM,[21,69,70] indicating that the detection range can effectively cover the physiological range of these biomarkers in sweat. Therefore, a wearable health monitor can be used to reliably detect concentrations of biomarkers in sweat.

Different light conditions can affect the color of bioassays captured by a camera, resulting in inaccurate concentration measurements.[29] Therefore, the color bar was placed on the health monitors as a reference to obtain a reliable concentration of biomarkers under different light conditions. Light influences the color of bioassays and the color bar simultaneously captured by a camera. Therefore, the existence of color reference can eliminate the interference of such environmental factors.[29] Figure S6A shows the images of color blocks with different *R*, *G*, and *B* values under different light conditions. The brightness of an adjustable bulb (Teckin SB50 Smart Alexa Light Bulb) was changed to obtain four different light conditions: 30, 50, 70, and 90% of maximum brightness. In addition, the color bar images under indoor light and sunlight were tested. According to the color detection results of different light conditions, although the *R* values of color blocks showed changes under the different light conditions, the *G* and *B* values of color blocks (Figure S6B−G) were not changed, indicating that there is no need to consider the impacts of *G* and *B* values on *R* values when having a color bar for color correction and white balance. Using the color bar as

https://doi.org/10.1021/acssensors.4c00528
ACS Sens. 2024, 9, 3212−3223

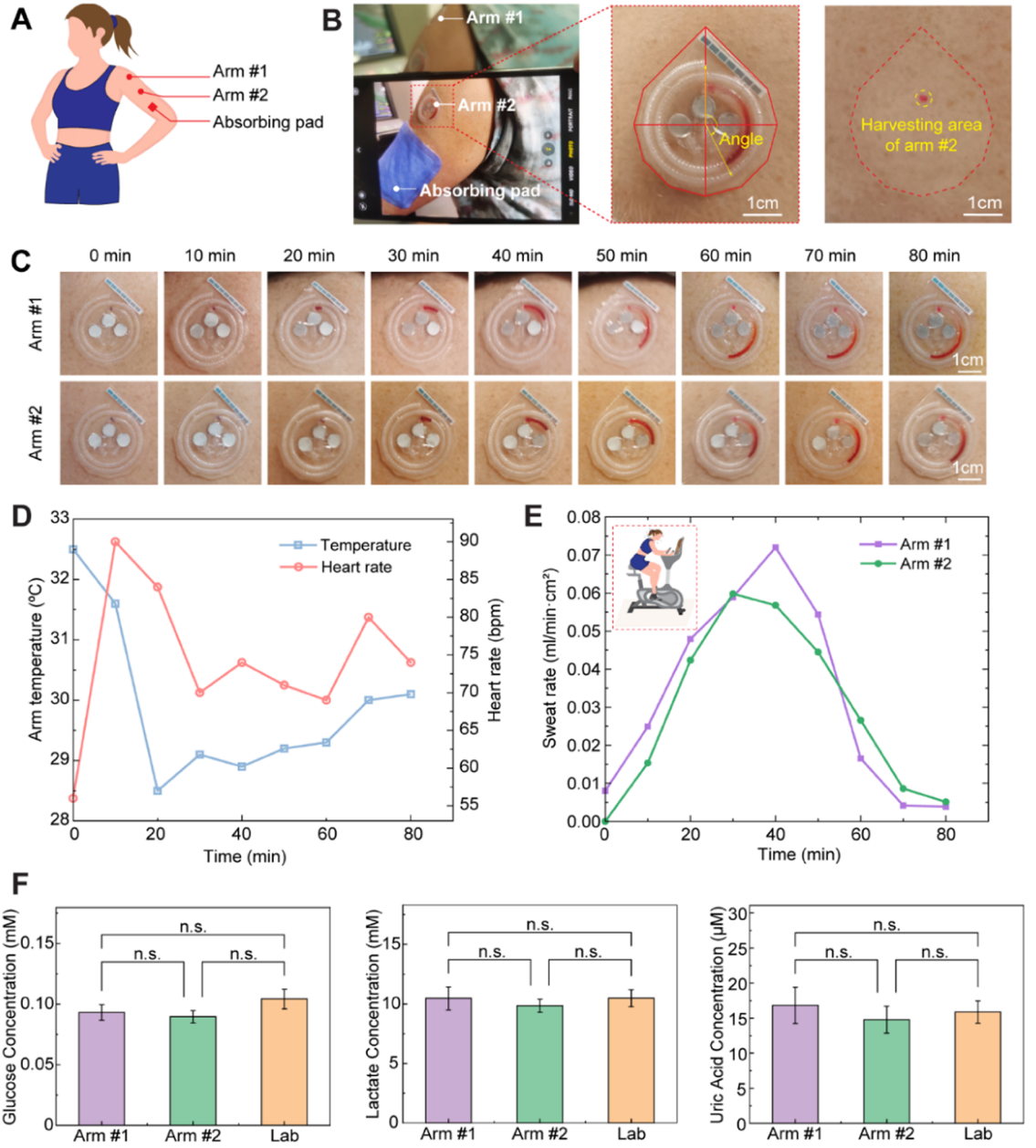

Figure 4. Feasibility study of sweat monitoring (68.9 °F, 59% humidity) through the 3D-printed wearable health monitors. (A) Schematic of body location for preliminary studies. (B) Optical images of application of the health monitors using a smartphone and quantification of the angle of filling front by ImageJ software. (C) Correlation of captured volume of sweat and the angle of filling front of the microfluidics. (D) Correlation of arm temperature and heart rate with time during the testing. (E) Correlation of sweat rate with time at two locations on the left arm. (F) Comparisons of concentration results of glucose, lactate, and uric acid via microfluidic health monitors and lab-based analysis (n.s.: no significant difference between the two results.).

the reference, the concentration detection results of biomarkers from health monitors under 5 different lighting conditions (20, 50, and 80% different brightness light intensities provided by adjustable brightness light bulb, indoor light, and sunlight light) are shown in Figure 2E−G. Glucose, lactate, and uric acid with standard concentrations were measured using the health monitors to determine the accuracy. Figure 2E−G shows that although the light conditions were different, the health monitors exhibited the capability to measure similar and relatively accurate biomarker concentrations. The results mentioned above indicate that the color bar method enables the elimination of the impact of light conditions and confirms the high accuracy of our health monitors.

Precise sweat rate monitoring confronts hindrances from skin contamination and sweat evaporation problems.[71] These issues can be addressed by developing skin-interfaced microfluidics to harvest and route sweat for controllable, continuous monitoring. Micron-scale channels present enhanced sensitivity for low sample volume.[72] The yield strength of silicone-based ink extruded layer-by-layer is sufficient to balance the gravity-induced bending moment via carefully designed filament stacking orientations in the submillimeter regime.[39]

Self-supporting structures (inner radius: 0.4−0.8 mm) and bottom layers (thickness: 0.45 mm) were drawn in AutoCAD

https://doi.org/10.1021/acssensors.4c00528
ACS Sens. 2024, 9, 3212−3223

software and then exported as stereolithography (.STL) files. The walls of the microfluidic channels (#M1 and #M2, thickness: 0.45 mm) printed layer-by-layer finally were merged at the top layers to form hollow channels, enabling self-supporting microfluidic structures. Figure 3A illustrates the 3D models of the designed self-supporting microfluidic component sliced by Slic3R software. Scanning electron microscopy (SEM) images in Figure 3B show that the self-supporting structures were successfully DIW-printed with pure silicone sealant inks without structural collapse and leakage. The inner radii of the cross sections were set from 0.3 to 0.8 mm. Depressions in the upper-left and upper-right corners of the semicircle set at 0.3 and 0.4 mm were observed in the cross section of SEM images (Figure 3B(a),(b)), while the central depression was found in the channels with a radius set to 0.5 mm. The air within the microfluidic channel follows the ideal gas law, so the flow impedance decreases as the cross-sectional area increases.[27] Considering the sweating rate, reaction time of bioassays, and usage time, we ultimately selected 0.6 and 0.4 mm as the inner radius settings for the spiral channel for measuring sweat rate and the central three channels connecting with the bioassays, respectively. After room temperature vulcanization, the volumes of microfluidic channels were measured by the syringe pump system setup pushing fluid at 0.5 mL/min (Figure 3C and Movie S2). The transparent test holder was printed with a stereolithography (SLA) printer using Formlabs clear resin. The whole support was hooked over the syringe pump, and an injection syringe containing red ink was mounted on the pump. The syringe needle was inserted from the inlet, and the red ink was injected through the outlet on the platform to the health monitors. When the inks for the microfluidic channels were fully cross-linked, the actual volume was reduced by about 40% for the 3D-printed channels with 0.3 and 0.4 mm settings and 20% for the inner radius above 0.6 mm compared to the theoretical values (Figure 3D). The correlation between the angle of the filling front and the corresponding volume from the inlet to the filling front point was also established via the syringe pump for the microfluidics (Figure 3E), which indicates that the angle of the filling front in the microfluidic channel can be used to calculate the volume of collected sweat. Young's modulus was calculated to be 430 kPa (silicone sealant) based on tensile tests (Figure S7A). The mechanical properties of our customized silicone-based polymeric inks (active agent: silicone agent; bulking agent: silicone grease) can be adjusted via increasing the ratio of bulking agents[73,74] for mounting the health monitor on different body locations (Figure S7A). The pure silicone-based polymeric ink exhibits superhydrophilicity with a water contact angle of ∼120° (Figure S7B). The correlation between the filling front of the spiral microfluidic channel and the volume is demonstrated in Figure 3E, which can be used to calculate the volume of captured human sweat in feasibility tests. The volume experienced rapid growth with the increase of the angle, and then the slope of the volume−angle curve decreased, eventually having a linear trend when the filling angle exceeded about 223°.

To evaluate on-body sweat sampling capabilities of our health monitors, preliminary feasibility studies for the sweat rate were performed on a healthy subject by riding an exercise bike at a room temperature of 68.9 °F and 59% humidity with two locations on the same arm (Figure 4A, Arm #1 and Arm #2). An absorbing pad was attached to the same arm to collect sweat for lab analysis of the three biomarkers (Figure 4A, absorbing pad). Optical images were taken every 10 min (Figure 4B), and the angle of the filling front of the health monitor was quantified by using ImageJ software. Clearly, no extra red liquid was observed outside the microfluidic zone during the testing and after the removal of health monitors, indicating that the sweat was successfully collected and routed into the channels without leakage issues. During physical activity, sweat flows into the four inlets of channels. The sweat rate within the three channels for bioassays (Figure 4C) was different during the feasibility studies, possibly due to the backpressure of the small channels and the distribution of sweat glands.[75] Bioassays of the health monitors at arm #1 and #2 locations had fully reacted with sweat for colorimetric sensing before the completion of our human studies. Thus, the images of sweat loss for the individual tests were sequentially collected (Figure 4C). Sweat rate was determined from the slope of the volume−time curve (Figure 3E). As shown in Figure 4D, during the exercise, the arm temperature dropped from 32.5 to 28.5 °C within the first 20 min, while the heart rate increased, going up from 56 to 90 bpm within the first 10 min. The two parameters show decreased fluctuation amplitude after 20 min in the testing period. In Figure 4E, from 30 to 40 min, the sweating rate of the two locations increased to the highest point about 0.07 and 0.06 mL/min·cm^2, respectively. The sweating rate decreased in response to the reduction of exercise intensity. The sweat rates of the two testing areas on the arm were roughly proportional to the distribution of sweat glands in the human body. It should be noted that the sweat rate varies among individuals and depends on the physiological conditions.[76] The feasibility studies tentatively verified the practical functions and prospective applications for outdoor exercising scenarios.

Field testing of sweat biomarkers using the health monitors on the arm of a healthy volunteer during cycling demonstrates the performance of the health monitors in an application. Figure S8 shows the health monitor on the arm before and after corrections of the color and white balance. Correction through a color checker can effectively improve the accuracy of the color of the images.[70] The difference in temperature and tint of the photo before and after correction is displayed in the lower right corner of Figure S8, which indicates that the color correction of the photo was completed. Figure 4F shows that there is no significant difference in the concentration of biomarkers in sweat measured using the health monitor and in the laboratory. The glucose concentration in sweat measured by the health monitor was about 0.086−0.100 mM. After collecting the individual sweat, the glucose concentration measured using a microplate reader was 0.095−0.111 mM. The bioassay detected the concentration of lactate in sweat ranging from 9.28 to 11.47 mM. According to the absorbance data from the microplate reader, the lactate concentration was determined as 9.71−11.14 mM. The result of uric acid in sweat from the field testing was from 13.03 to 18.88 μM. In the laboratory, the concentration of uric acid in sweat was 14.87−17.73 μM. Compared with biomarkers concentrations in normal human sweat and previous similar studies,[29,77,78] the concentrations of three biomarkers were within the normal range. The difference between the glucose concentration at two points on the volunteer's arm measured by the health monitor and the glucose concentration measured in the laboratory was 0.011−0.015 mM. The differences between the health monitor and laboratory measurements for lactate and uric acid were 0.03−0.63 mM and 0.94−1.10 μM, respectively.

https://doi.org/10.1021/acssensors.4c00528
ACS Sens. 2024, 9, 3212−3223

The disparity between health monitor testing results and laboratory analysis in this study is lower than in previous similar studies that used commercial enzymes instead of Fe−N−C SACs in health monitors for glucose.[10,29] Similarly, the disparity between the health monitor test and laboratory analysis of lactate measurement in this study (0.030−0.63 mM) is also lower than in similar studies that applied commercial enzymes to measure lactate concentration in human sweat.[29] The comparison results reflect the high sensitivity of Fe−N−C SACs as peroxidases and the accuracy of SACs-based bioassays.

CONCLUSIONS

In summary, this work introduces a proof-of-concept for a disposable 3D-printed wearable, flexible health monitor equipped with self-supporting microfluidics for monitoring sweat rate and colorimetric sensing of glucose, lactate, and uric acid. The *in situ* sampling process within self-supporting microfluidics minimizes sweat evaporation and contamination. The sensitivity of biomarker detection based on enzymatic reactions is enhanced by employing SACs-based bioassays. The feasibility study of the health monitors on human skin has effectively validated that the combination of one-step fabrication via 3D printing and novel sensitive nanomaterials enables noninvasive monitoring of sweat rate and biomarker concentrations. This is crucial for evaluating athletic performance and physiological conditions, contributing to the development of the next generation of fully integrated wearable sweat health monitors. Future studies will focus on developing image processing and colorimetric analysis applications for smartphones, exploring the potentials of additive manufacturing in three key areas: (1) integrating capillary valves and pumps for continuous monitoring, (2) investigating reusable wearable health monitors for long-term use, and (3) enhancing real-time analysis capabilities with smartphone applications. Overall, our work demonstrates the feasibility of 3D-printed flexible wearable health monitors for health monitoring.

EXPERIMENTAL SECTION

Ink Materials for 3D Printing. Silicone-based polymeric inks (acetoxy-based RTV sealant Loctite SI 595 CL) were loaded into a Nordson EFD - HP 7× High-Pressure Dispensing Tool (3 cm^3 barrels) for direct ink writing. Food-grade red dye was used at the inlet region of microfluidics for visualization, and 3M 1524 Medical Transfer Adhesive was used as a adhesive layer.

Preparation of SACs-Based Colorimetric Bioassays. The immersing absorbent paper (Whatman grade 3MM) was fabricated for small bioassays with a diameter of 6.4 mm as the reaction zones in the health monitor. The bioassays were put one by one into the wells of a 96-well plate (Celltreat 96-Well Polystyrene Cell Culture Non-Treated Plates). Next, Fe−N−C SACs were ground carefully in a mortar and dispersed in ethyl alcohol to form a 1 mg/mL Fe−N−C SACs suspension. Then, 5 μL of a 1 mg/mL Fe−N−C SACs suspension was slowly dropped onto each bioassay to ensure even distribution on bioassays. GOx, LOX, and UOX were dissolved in phosphate-buffered saline (PBS), respectively, to prepare three enzyme solutions. The concentration of GOx and LOX is 1 mg/mL, and the concentration of UOX is 0.5 mg/mL. Five μL of GOx, LOX, and UOX solutions were dropped onto the bioassays for detecting glucose, lactate, and uric acid, respectively. Finally, three types of detected bioassays were obtained after drying. All of the above drying processes were carried out in a 37 °C incubator. The bioassays were stored at 4 °C without exposure to light. The bioassays were placed on a plate that was fabricated with the same material as the health monitor to detect the sensing function of 3 types of bioassays. Glucose solutions of different concentrations were simultaneously injected via a different channel using a pipet to simulate the inflow of sweat via the microfluidic channel in the health monitor. After 5 min, the images of the bioassays were taken with a camera (Nikon D750, MACRO 105 mm F2.8 EX DG OS HSM, SIGMA) from ∼20 cm above. After color calibration and white balance calibration using a color checker (ColorChecker Passport Photo 2, Calibrate) and Adobe Lightroom software (Adobe Inc., San Jose, CA), the reliable *R*, *G*, and *B* values of color were obtained by ImageJ software. The same method was used to detect lactate and uric acid.

Preparation of Color Reference and Color Analysis Using Color Reference. Color blocks with different *R*, *G*, and *B* values were printed on paper to determine the effect of different *G* and *B* values of the color reference and various light sources on the *R* value. Figure S5A shows the *R* (130, 110, 90, 70, 50), *G* (120, 100, 80), and *B* (120, 100, 80) values of the color blocks. By adjusting the brightness of the light bulb, the images of color blocks with different brightnesses (30, 50, 70, and 90%) were taken by the camera. The two images were taken under indoor and sunlight lighting conditions. After the color and white balance correction, images captured by the camera with different light sources were measured *R* values by using ImageJ (Figure S5B−G). Seven color blocks with different *R* values are printed on paper to form a color reference. The *R* values of the color blocks are 60, 70, 80, 90, 100, 110, and 120. The concentrations of biomarkers corresponding to each color block are listed in Table S2. Five μL of various concentrations of glucose (0.2, 0.1, 0.05, and 0.02 mM) were added to the bioassay through the channel. The photos of the bioassay and color reference were taken by camera after 5 min. The calibration curve with different light sources was obtained to get the concentration of glucose on the bioassay. The same method was used to measure the concentrations of lactate and uric acid. The concentrations of lactate solution were 50, 30, 10, and 1 mM, and the concentrations of uric acid solution were 80, 60, 40, and 20 μM.

Fabrication of Flexible Wearable Health Monitors by Direct Ink Writing and Pick-and-Place Strategy. The one-step printing was performed on a customized 3D-printing system (AGS1000, Aerotech) with three independent motion-controlled axes. The G-code indicating printing paths was generated by slicing the .STL files were prepared with open-source Slic3r software. Three high-precision dispensers (Ultimus V and Nordson EFD) were used simultaneously. The first dispenser was used for the extrusion of inks through direct ink writing (DIW) with pressure mode (inner diameter of nozzle: 0.15 mm, pressure: 3500 kPa, speed: 8−10 mm/s). The second dispenser was used for automated place-and-place via an empty barrel with moderate vacuum mode (nozzle: 1.65 mm, pressure: 10 ″H_2O (vacuum) and 8 kPa (release the bioassays, speed: 1 mm/s)). The vacuum mode was activated once the nozzle was moved to the initial location of the bioassays. The paper-based bioassays were lifted, transferred, and deposited at target positions one by one. The three bioassays were covered by transparent and flexible PU films to prevent a reaction with the air. The third dispenser (nozzle: 0.2 mm, pressure: 30 kPa, speed: 1 mm/s) was used for adding the red dye to the designated location near the inlet of the spiral microfluidic channel.

Validation of the Relationship Between Filling Angle and Volume in Microfluidics. The relation between filling angle and volume was established by pumping water through a syringe pump into 3D-printed health monitors at a constant flow speed of 0.5 mL/min.

Characterization. The polymeric ink with different weight ratios of bulking agent (silicone grease #LP20, Trident) to the active agent (acetoxy-based RTV sealant Loctite SI 595 CL) was printed into rectangular samples (dimensions (length × width × thickness): 35 mm × 5 mm × 1 mm). The tensile tests were performed using a mechanical analyzer (Mark-10 Tensile Force Testers). The contact angle of the cured silicone-based polymeric substrate was characterized by using a VCA-OPTIMA system. Images were taken immediately after dispensing 1 μL droplets of deionized water. SEM images of microfluidic channels (sputter coated with gold) were obtained using an FEI SEM Apreo Volumescope with EDAX and

https://doi.org/10.1021/acssensors.4c00528
ACS Sens. 2024, 9, 3212−3223

EBSD detectors at an accelerating voltage of 10 kV. The volume of microfluidic channels was measured by a syringe pump system (NE-1000 One Channel Programmable Syringe Pump). The Fe−N−C SACs characterization was performed using transmission electron microscopy (FEI Tecnai G2 20 Twin TEM, 200 kV LaB6 electron source). Fe−N−C SACs were dispersed in ethanol to obtain 3 and 0.3 mg/mL SAC solutions. The morphology of Fe−N−C SACs in both solutions was observed using TEM. The HAADF-STEM imaging was conducted on a Hitachi HD2700C STEM operated at 200 kV and equipped with a probe aberration corrector (spatial resolution <1 Å, energy resolution 0.35 eV). The collection angle for HAADF is between 64 and 341 mad.

Feasibility Study of Microfluidic Health Monitors on Human Skin. The feasibility study of microfluidic health monitors on human skin was conducted on a healthy subject. An IRB review at the Washington State University determined that this experiment does not meet the federal definition of human subjects research, and therefore, an IRB review was not required. The tests were performed on an Expresso GO Upright exercise bike in the gym at Washington State University (68.9 °F; 59% humidity). After the skin was cleaned with alcohol wipes, flexible wearable health monitors were attached to the two body locations (Arm #1 and Arm #2). Optical images were captured every 10 min and quantified by ImageJ software to obtain the filling angles. After the field test, the color checker was placed next to the health monitor, and the color change of the bioassay in the health monitors and color checker were recorded together (Figure S8). After the color correction and white balance correction of Adobe Lightroom software (Adobe Inc., San Jose, CA), the *R* values of the bioassays were obtained. At the same time, the *R* values of color blocks on the color reference were recorded to obtain the calibration curve that was used to obtain the concentration of biomarkers from the *R* values of bioassays. Then, the sweat collected by the health monitors was used to verify the biomarker concentration in the laboratory. The concentrations of the biomarkers were determined by a standard and conventional biomarker concentration determination method with a microplate reader.[79] Five μL portion of sweat and biomarkers of different concentrations were added to the well of a 96-well plate, followed by 10 μL of 1 mg/mL Fe−N−C SACs, 30 μL of oxidase (GOx, LOX, or UOX), and 50 μL of TMB. After incubating at 37 °C for 5 min, the plate was read using a microplate reader, and the absorbances of wells were measured at a wavelength of 370 nm. The data was used to establish a linear relationship between biomarker concentrations and standard solution absorbance, enabling the calculation of biomarker concentrations in sweat. Finally, the measurement accuracy of the health monitor was conducted by comparing the concentration of biomarkers on the health monitor with those measured in the laboratory.

■ ASSOCIATED CONTENT

Supporting Information

The Supporting Information is available free of charge at https://pubs.acs.org/doi/10.1021/acssensors.4c00528.

Additional experimental details, including materials and methods; finite element analysis of the microfluidic structure; fabrication of Fe−N−C SACs through synthesis and pyrolysis at 950°C; characterization of Fe−N−C SACs; comparison of detection linear range and limit of detection (LOD) of wearable sensors for detecting biomarkers in sweat; concentrations of the biomarker corresponding to the *R* values (PDF)

3D-printing process for the health monitor (Movie S1) (MP4)

Experimental setup for testing of the microfluidic channel (Movie S2) (MP4)

■ AUTHOR INFORMATION

Corresponding Authors

Dan Du − *School of Mechanical and Materials Engineering, Washington State University, Pullman, Washington 99164, United States;* orcid.org/0000-0003-1952-4042; Email: annie.du@wsu.edu

Kaiyan Qiu − *School of Mechanical and Materials Engineering, Washington State University, Pullman, Washington 99164, United States;* orcid.org/0000-0002-3138-0275; Email: kaiyan.qiu@wsu.edu

Authors

Chuchu Chen − *School of Mechanical and Materials Engineering, Washington State University, Pullman, Washington 99164, United States;* orcid.org/0009-0005-3578-8517

Yonghao Fu − *School of Mechanical and Materials Engineering, Washington State University, Pullman, Washington 99164, United States*

Sonja S. Sparks − *School of Mechanical and Materials Engineering, Washington State University, Pullman, Washington 99164, United States*

Zhaoyuan Lyu − *School of Mechanical and Materials Engineering, Washington State University, Pullman, Washington 99164, United States;* orcid.org/0000-0003-0888-8297

Arijit Pradhan − *School of Mechanical and Materials Engineering, Washington State University, Pullman, Washington 99164, United States*

Shichao Ding − *School of Mechanical and Materials Engineering, Washington State University, Pullman, Washington 99164, United States*

Narasimha Boddeti − *School of Mechanical and Materials Engineering, Washington State University, Pullman, Washington 99164, United States*

Yun Liu − *Research School of Chemistry, Australian National University, Canberra, ACT 2601, Australia*

Yuehe Lin − *School of Mechanical and Materials Engineering, Washington State University, Pullman, Washington 99164, United States;* orcid.org/0000-0003-3791-7587

Complete contact information is available at: https://pubs.acs.org/10.1021/acssensors.4c00528

Author Contributions

Conceptualization: K.Q., D.D., Y.L. C.C., Y.F, Z.L, Y.L., and SD. Methodology: K.Q., D.D., Y.L., C.C., and Y.F. Investigation: C.C., Y.F., S.S.S., and A.P. Visualization: C.C., Y.F., S.S.S., and A.P. Writing—original draft: C.C., Y.F., and A.P. Writing—review and editing: K.Q., Y.L., D.D., Y.L., and N.B. Funding Acquisition: K.Q. and D.D. Project supervision: K.Q., D.D., and Y.L.

Notes

The authors declare no competing financial interest.

■ ACKNOWLEDGMENTS

Prof. Kaiyan Qiu acknowledges WSU Startup Funds, WSU Commercialization Special Funds, and National Science Foundation (DGE #2244082). Prof. Dan Du acknowledges the Centers for Disease Control and Prevention/National Institute for Occupational Safety and Health (CDC/NIOSH) grant (1 R01OH012579-01-00). Prof. Yun Liu acknowledges the funding support of the Australian Research Council in the

form of Discovery Project (DP200100159, FL210100017). The authors thank John P. Swensen and Amit Bandyopadhyay in Dana Building at WSU for mechanical test support and contact angle test support, respectively. The authors thank the characterization support from Franceschi Microscopy and Imaging Center (FMIC) at WSU. The authors also thank Alejandro G. Obando for the valuable suggestions for the paper.

REFERENCES

(1) Ji, W.; Zhu, J.; Wu, W.; Wang, N.; Wang, J.; Wu, J.; Wu, Q.; Wang, X.; Yu, C.; Wei, G.; et al. Wearable Sweat Biosensors Refresh Personalized Health/Medical Diagnostics. *Research* **2021**, *2021*, No. 9757126.
(2) Kim, J.; Campbell, A. S.; de Avila, B. E.; Wang, J. Wearable biosensors for healthcare monitoring. *Nat. Biotechnol.* **2019**, *37* (4), 389−406.
(3) Bariya, M.; Nyein, H. Y. Y.; Javey, A. Wearable sweat sensors. *Nat. Electron.* **2018**, *1* (3), 160−171.
(4) Dunn, J.; Runge, R.; Snyder, M. Wearables and the medical revolution. *Pers. Med.* **2018**, *15* (5), 429−448.
(5) Yang, Y.; Gao, W. Wearable and flexible electronics for continuous molecular monitoring. *Chem. Soc. Rev.* **2019**, *48* (6), 1465−1491.
(6) Yu, H. X.; Sun, J. T. Sweat detection theory and fluid driven methods: A review. *Nanotechnol. Precis. Eng.* **2020**, *3* (3), 126−140.
(7) Yang, D. S.; Ghaffari, R.; Rogers, J. A. Sweat as a diagnostic biofluid. *Science* **2023**, *379* (6634), 760−761.
(8) Tsierkezos, N. G.; Othman, S. H.; Ritter, U.; Hafermann, L.; Knauer, A.; Köhler, J. M.; Downing, C.; McCarthy, E. K. Electrochemical analysis of ascorbic acid, dopamine, and uric acid on nobel metal modified nitrogen-doped carbon nanotubes. *Sens. Actuators, B* **2016**, *231*, 218−229.
(9) Emaminejad, S.; Gao, W.; Wu, E.; Davies, Z. A.; Nyein, H. Y. Y.; Challa, S.; Ryan, S. P.; Fahad, H. M.; Chen, K.; Shahpar, Z.; et al. Autonomous sweat extraction and analysis applied to cystic fibrosis and glucose monitoring using a fully integrated wearable platform. *Proc. Natl. Acad. Sci. U.S.A.* **2017**, *114* (18), 4625−4630.
(10) Xiao, J.; Liu, Y.; Su, L.; Zhao, D.; Zhao, L.; Zhang, X. Microfluidic Chip-Based Wearable Colorimetric Sensor for Simple and Facile Detection of Sweat Glucose. *Anal. Chem.* **2019**, *91* (23), 14803−14807.
(11) Yang, Y.; Song, Y.; Bo, X.; Min, J.; Pak, O. S.; Zhu, L.; Wang, M.; Tu, J.; Kogan, A.; Zhang, H.; et al. A laser-engraved wearable sensor for sensitive detection of uric acid and tyrosine in sweat. *Nat. Biotechnol.* **2020**, *38* (2), 217−224.
(12) Van Hoovels, K.; Xuan, X.; Cuartero, M.; Gijssel, M.; Swarén, M.; Crespo, G. A. Can wearable sweat lactate sensors contribute to sports physiology? *ACS Sens.* **2021**, *6* (10), 3496−3508.
(13) Nyein, H. Y. Y.; Tai, L. C.; Ngo, Q. P.; Chao, M.; Zhang, G. B.; Gao, W.; Bariya, M.; Bullock, J.; Kim, H.; Fahad, H. M.; Javey, A. A Wearable Microfluidic Sensing Patch for Dynamic Sweat Secretion Analysis. *ACS Sens.* **2018**, *3* (5), 944−952.
(14) Wei, L.; Lv, Z. H.; He, Y. X.; Cheng, L.; Qiu, Y.; Huang, X. Z.; Ding, C.; Wu, H. P.; Liu, A. P. In-situ admittance sensing of sweat rate and chloride level in sweat using wearable skin-interfaced microfluidic patch. *Sens. Actuators, B* **2023**, *379*, No. 133213.
(15) Mohan, A. M. V.; Rajendran, V.; Mishra, R. K.; Jayaraman, M. Recent advances and perspectives in sweat based wearable electrochemical sensors. *TrAC, Trends Anal. Chem.* **2020**, *131*, No. 116024.
(16) Xu, J.; Fang, Y.; Chen, J. Wearable Biosensors for Non-Invasive Sweat Diagnostics. *Biosensors* **2021**, *11* (8), No. 245, DOI: 10.3390/bios11080245.
(17) Moyer, J.; Wilson, D.; Finkelshtein, I.; Wong, B.; Potts, R. Correlation Between Sweat Glucose and Blood Glucose in Subjects with Diabetes. *Diabetes Technol. Ther.* **2012**, *14* (5), 398−402.
(18) Xie, X.; Wang, D. P.; Guo, C.; Liu, Y.; Rao, Q.; Lou, F.; Li, Q.; Dong, Y.; Li, Q.; Yang, H. B.; Hu, F. X. Single-Atom Ruthenium Biomimetic Enzyme for Simultaneous Electrochemical Detection of Dopamine and Uric Acid. *Anal. Chem.* **2021**, *93* (11), 4916−4923.
(19) Baker, L. B.; Wolfe, A. S. Physiological mechanisms determining eccrine sweat composition. *Eur. J. Appl. Physiol.* **2020**, *120* (4), 719−752.
(20) Zhang, K.; Zhang, J.; Wang, F.; Kong, D. Stretchable and Superwettable Colorimetric Sensing Patch for Epidermal Collection and Analysis of Sweat. *ACS Sens.* **2021**, *6* (6), 2261−2269.
(21) Zhong, B.; Jiang, K.; Wang, L.; Shen, G. Wearable Sweat Loss Measuring Devices: From the Role of Sweat Loss to Advanced Mechanisms and Designs. *Adv. Sci.* **2022**, *9* (1), No. e2103257.
(22) Sawka, M. N. Physiological consequences of hypohydration: exercise performance and thermoregulation. *Med. Sci. Sports Exercise* **1992**, *24* (6), 657−670.
(23) Maughan, R. J. Impact of mild dehydration on wellness and on exercise performance. *Eur. J. Clin. Nutr.* **2003**, *57* (2), S19−S23.
(24) Korpelainen, J. T.; Sotaniemi, K. A.; Myllyla, V. V. Hyperhidrosis as a reflection of autonomic failure in patients with acute hemispheral brain infarction. An evaporimetric study. *Stroke* **1992**, *23* (9), 1271−1275.
(25) Zhao, H.; Zhang, X.; Qin, Y.; Xia, Y.; Xu, X.; Sun, X.; Yu, D.; Mugo, S. M.; Wang, D.; Zhang, Q. An integrated wearable sweat sensing patch for passive continuous analysis of stress biomarkers at rest. *Adv. Funct. Mater.* **2023**, *33* (9), No. 2212083.
(26) Heikenfeld, J.; Jajack, A.; Feldman, B.; Granger, S. W.; Gaitonde, S.; Begtrup, G.; Katchman, B. A. Accessing analytes in biofluids for peripheral biochemical monitoring. *Nat. Biotechnol.* **2019**, *37* (4), 407−419.
(27) Koh, A.; Kang, D.; Xue, Y.; Lee, S.; Pielak, R. M.; Kim, J.; Hwang, T.; Min, S.; Banks, A.; Bastien, P.; et al. A soft, wearable microfluidic device for the capture, storage, and colorimetric sensing of sweat. *Sci. Transl. Med.* **2016**, *8* (366), No. 366ra165.
(28) Mei, X.; Yang, J.; Liu, J.; Li, Y. Wearable, nanofiber-based microfluidic systems with integrated electrochemical and colorimetric sensing arrays for multiplex sweat analysis. *Chem. Eng. J.* **2023**, *454*, No. 140248.
(29) Choi, J.; Bandodkar, A. J.; Reeder, J. T.; Ray, T. R.; Turnquist, A.; Kim, S. B.; Nyberg, N.; Hourlier-Fargette, A.; Model, J. B.; Aranyosi, A. J.; et al. Soft, Skin-Integrated Multifunctional Microfluidic Systems for Accurate Colorimetric Analysis of Sweat Biomarkers and Temperature. *ACS Sens.* **2019**, *4* (2), 379−388.
(30) Liu, S.; Yang, D. S.; Wang, S.; Luan, H.; Sekine, Y.; Model, J. B.; Aranyosi, A. J.; Ghaffari, R.; Rogers, J. A. Soft, environmentally degradable microfluidic devices for measurement of sweat rate and total sweat loss and for colorimetric analysis of sweat biomarkers. *EcoMat* **2023**, *5* (1), No. e12270.
(31) Wu, C. H.; Ma, H. J. H.; Baessler, P.; Balanay, R. K.; Ray, T. R. Skin-interfaced microfluidic systems with spatially engineered 3D fluidics for sweat capture and analysis. *Sci. Adv.* **2023**, *9* (18), No. eadg4272.
(32) Brothers, M. C.; DeBrosse, M.; Grigsby, C. C.; Naik, R. R.; Hussain, S. M.; Heikenfeld, J.; Kim, S. S. Achievements and Challenges for Real-Time Sensing of Analytes in Sweat within Wearable Platforms. *Acc. Chem. Res.* **2019**, *52* (2), 297−306.
(33) Lee, H.; Song, C.; Hong, Y. S.; Kim, M.; Cho, H. R.; Kang, T.; Shin, K.; Choi, S. H.; Hyeon, T.; Kim, D. H. Wearable/disposable sweat-based glucose monitoring device with multistage transdermal drug delivery module. *Sci. Adv.* **2017**, *3* (3), No. e1601314.
(34) Shirreffs, S. M.; Maughan, R. J. Whole body sweat collection in humans: an improved method with preliminary data on electrolyte content. *J. Appl. Physiol.* **1997**, *82* (1), 336−341.
(35) Matzeu, G.; Fay, C.; Vaillant, A.; Coyle, S.; Diamond, D. A Wearable Device for Monitoring Sweat Rates via Image Analysis. *IEEE Trans. Biomed. Eng.* **2016**, *63* (8), 1672−1680.
(36) Min, J.; Tu, J.; Xu, C.; Lukas, H.; Shin, S.; Yang, Y.; Solomon, S. A.; Mukasa, D.; Gao, W. Skin-Interfaced Wearable Sweat Sensors for Precision Medicine. *Chem. Rev.* **2023**, *123* (8), 5049−5138.
(37) Heikenfeld, J.; Jajack, A.; Rogers, J.; Gutruf, P.; Tian, L.; Pan, T.; Li, R.; Khine, M.; Kim, J.; Wang, J.; Kim, J. Wearable sensors:

modalities, challenges, and prospects. *Lab Chip* **2018**, *18* (2), 217−248.
(38) Bandodkar, A. J.; Gutruf, P.; Choi, J.; Lee, K.; Sekine, Y.; Reeder, J. T.; Jeang, W. J.; Aranyosi, A. J.; Lee, S. P.; Model, J. B.; et al. Battery-free, skin-interfaced microfluidic/electronic systems for simultaneous electrochemical, colorimetric, and volumetric analysis of sweat. *Sci. Adv.* **2019**, *5* (1), No. eaav3294.
(39) Su, R.; Wen, J.; Su, Q.; Wiederoder, M. S.; Koester, S. J.; Uzarski, J. R.; McAlpine, M. C. 3D printed self-supporting elastomeric structures for multifunctional microfluidics. *Sci. Adv.* **2020**, *6* (41), No. eabc9846.
(40) Ates, H. C.; Nguyen, P. Q.; Gonzalez-Macia, L.; Morales-Narvaez, E.; Guder, F.; Collins, J. J.; Dincer, C. End-to-end design of wearable sensors. *Nat. Rev. Mater.* **2022**, *7* (11), 887−907.
(41) Hassan, M.; Abbas, G.; Li, N.; Afzal, A.; Haider, Z.; Ahmed, S.; Xu, X.; Pan, C.; Peng, Z. Significance of flexible substrates for wearable and implantable devices: recent advances and perspectives. *Adv. Mater. Technol.* **2022**, *7* (3), No. 2100773.
(42) Lim, H. R.; Kim, H. S.; Qazi, R.; Kwon, Y. T.; Jeong, J. W.; Yeo, W. H. Advanced Soft Materials, Sensor Integrations, and Applications of Wearable Flexible Hybrid Electronics in Healthcare, Energy, and Environment. *Adv. Mater.* **2020**, *32* (15), No. e1901924.
(43) Kant, R.; Chauhan, P. S.; Patel, V. K.; Bhattacharya, S.Introduction to the Fabrication of Polymers and Polymeric Composites. In *Trends in Fabrication of Polymers and Polymer Composites*; AIP Publishing, 2022; pp 1−10.
(44) Loke, G.; Yuan, R.; Rein, M.; Khudiyev, T.; Jain, Y.; Joannopoulos, J.; Fink, Y. Structured multimaterial filaments for 3D printing of optoelectronics. *Nat. Commun.* **2019**, *10* (1), No. 4010.
(45) Dhinesh, S. K.; Kumar, K. L. S. A Review on 3D Printed Sensors. *IOP Conf. Ser.: Mater. Sci. Eng.* **2020**, *764*, No. 012055, DOI: 10.1088/1757-899X/764/1/012055.
(46) Raoufi, M. A.; Bazaz, S. R.; Niazmand, H.; Rouhi, O.; Asadnia, M.; Razmjou, A.; Warkiani, M. E. Fabrication of unconventional inertial microfluidic channels using wax 3D printing. *Soft Matter* **2020**, *16* (10), 2448−2459.
(47) Ghaznavi, A.; Xu, J.; Hara, S. A. A Non-Sacrificial 3D Printing Process for Fabricating Integrated Micro/Mesoscale Molds. *Micromachines* **2023**, *14* (7), No. 1363, DOI: 10.3390/mi14071363.
(48) Gross, B. C.; Anderson, K. B.; Meisel, J. E.; McNitt, M. I.; Spence, D. M. Polymer Coatings in 3D-Printed Fluidic Device Channels for Improved Cellular Adherence Prior to Electrical Lysis. *Anal. Chem.* **2015**, *87* (12), 6335−6341.
(49) Ornelas-González, A.; González-González, M.; Rito-Palomares, M. Development of a simple and flexible enzyme-based platform for the colorimetric detection of multiple biomarkers in non-conventional biofluids. *J. Chem. Technol. Biotechnol.* **2022**, *97* (8), 1959−1965.
(50) Jeon, H. J.; Kim, H. S.; Chung, E.; Lee, D. Y. Nanozyme-based colorimetric biosensor with a systemic quantification algorithm for noninvasive glucose monitoring. *Theranostics* **2022**, *12* (14), 6308−6338.
(51) Zhu, D.; Liu, B.; Wei, G. Two-Dimensional Material-Based Colorimetric Biosensors: A Review. *Biosensors* **2021**, *11*, No. 259, DOI: 10.3390/bios11080259.
(52) Qian, S.; Cui, Y.; Cai, Z.; Li, L. Applications of smartphone-based colorimetric biosensors. *Biosens. Bioelectron.: X* **2022**, *11*, No. 100173.
(53) Niu, X.; Li, X.; Lyu, Z.; Pan, J.; Ding, S.; Ruan, X.; Zhu, W.; Du, D.; Lin, Y. Metal-organic framework based nanozymes: promising materials for biochemical analysis. *Chem. Commun.* **2020**, *56* (77), 11338−11353.
(54) Wu, J.; Wang, X.; Wang, Q.; Lou, Z.; Li, S.; Zhu, Y.; Qin, L.; Wei, H. Nanomaterials with enzyme-like characteristics (nanozymes): next-generation artificial enzymes (II). *Chem. Soc. Rev.* **2019**, *48* (4), 1004−1076.
(55) Jiao, L.; Yan, H. Y.; Wu, Y.; Gu, W. L.; Zhu, C. Z.; Du, D.; Lin, Y. H. When Nanozymes Meet Single-Atom Catalysis. *Angew. Chem., Int. Ed.* **2020**, *59* (7), 2565−2576.
(56) Wu, W.; Huang, L.; Wang, E.; Dong, S. Atomic engineering of single-atom nanozymes for enzyme-like catalysis. *Chem. Sci.* **2020**, *11* (36), 9741−9756.
(57) Zhang, X. Y.; Chen, P. F.; He, S. W. X.; Jiang, B. W.; Wang, Y.; Cheng, Y. H.; Peng, J.; Verpoort, F.; Wang, J. H.; Kou, Z. K. Single-atom metal-nitrogen-carbon catalysts energize single molecule detection for biosensing. *InfoMat* **2023**, *5* (6), No. e12421.
(58) Lyu, Z.; Ding, S.; Zhang, N.; Zhou, Y.; Cheng, N.; Wang, M.; Xu, M.; Feng, Z.; Niu, X.; Cheng, Y.; et al. Single-Atom Nanozymes Linked Immunosorbent Assay for Sensitive Detection of Abeta 1−40: A Biomarker of Alzheimer's Disease. *Research* **2020**, *2020*, No. 4724505.
(59) Niu, X.; Shi, Q.; Zhu, W.; Liu, D.; Tian, H.; Fu, S.; Cheng, N.; Li, S.; Smith, J. N.; Du, D.; Lin, Y. Unprecedented peroxidase-mimicking activity of single-atom nanozyme with atomically dispersed Fe-N(x) moieties hosted by MOF derived porous carbon. *Biosens. Bioelectron.* **2019**, *142*, No. 111495.
(60) Cheng, N.; Li, J. C.; Liu, D.; Lin, Y.; Du, D. Single-Atom Nanozyme Based on Nanoengineered Fe-N-C Catalyst with Superior Peroxidase-Like Activity for Ultrasensitive Bioassays. *Small* **2019**, *15* (48), No. e1901485.
(61) Valentine, A. D.; Busbee, T. A.; Boley, J. W.; Raney, J. R.; Chortos, A.; Kotikian, A.; Berrigan, J. D.; Durstock, M. F.; Lewis, J. A. Hybrid 3D Printing of Soft Electronics. *Adv. Mater.* **2017**, *29* (40), No. 1703817.
(62) Zhu, Z.; Guo, S. Z.; Hirdler, T.; Eide, C.; Fan, X.; Tolar, J.; McAlpine, M. C. 3D Printed Functional and Biological Materials on Moving Freeform Surfaces. *Adv. Mater.* **2018**, *30* (23), No. e1707495.
(63) Schulz, I. J. Micropuncture studies of the sweat formation in cystic fibrosis patients. *J. Clin. Invest.* **1969**, *48* (8), 1470−1477.
(64) Baker, L. B.; Model, J. B.; Barnes, K. A.; Anderson, M. L.; Lee, S. P.; Lee, K. A.; Brown, S. D.; Reimel, A. J.; Roberts, T. J.; Nuccio, R. P.; et al. Skin-interfaced microfluidic system with personalized sweating rate and sweat chloride analytics for sports science applications. *Sci. Adv.* **2020**, *6* (50), No. eabe3929.
(65) Reeder, J. T.; Choi, J.; Xue, Y.; Gutruf, P.; Hanson, J.; Liu, M.; Ray, T.; Bandodkar, A. J.; Avila, R.; Xia, W.; et al. Waterproof, electronics-enabled, epidermal microfluidic devices for sweat collection, biomarker analysis, and thermography in aquatic settings. *Sci. Adv.* **2019**, *5* (1), No. eaau6356.
(66) Lee, C. H.; Ma, Y. J.; Jang, K. I.; Banks, A.; Pan, T.; Feng, X.; Kim, J. S.; Kang, D.; Raj, M. S.; McGrane, B. L.; et al. Soft Core/Shell Packages for Stretchable Electronics. *Adv. Funct. Mater.* **2015**, *25* (24), 3698−3704.
(67) Niu, X.; Shi, Q.; Zhu, W.; Liu, D.; Tian, H.; Fu, S.; Cheng, N.; Li, S.; Smith, J. N.; Du, D.; Lin, Y. Unprecedented peroxidase-mimicking activity of single-atom nanozyme with atomically dispersed Fe−Nx moieties hosted by MOF derived porous carbon. *Biosens. Bioelectron.* **2019**, *142*, No. 111495.
(68) Teekayupak, K.; Ruecha, N.; Chailapakul, O.; Rodthongkum, N. Flexible cotton-AuNP thread electrode for non-enzymatic sensor of uric acid in urine. *Cellulose* **2021**, *28* (16), 10501−10515.
(69) Xiao, J.; Luo, Y.; Su, L.; Lu, J.; Han, W.; Xu, T.; Zhang, X. Hydrophilic metal-organic frameworks integrated uricase for wearable detection of sweat uric acid. *Anal. Chim. Acta* **2022**, *1208*, No. 339843.
(70) Cheng, Y.; Feng, S.; Ning, Q.; Li, T.; Xu, H.; Sun, Q.; Cui, D.; Wang, K. Dual-signal readout paper-based wearable biosensor with a 3D origami structure for multiplexed analyte detection in sweat. *Microsyst. Nanoeng.* **2023**, *9* (1), No. 36, DOI: 10.1038/s41378-023-00514-2.
(71) He, X.; Fan, C.; Luo, Y.; Xu, T.; Zhang, X. Flexible microfluidic nanoplasmonic sensors for refreshable and portable recognition of sweat biochemical fingerprint. *npj Flexible Electron.* **2022**, *6*, No. 60, DOI: 10.1038/s41528-022-00192-6.
(72) Sonner, Z.; Wilder, E.; Heikenfeld, J.; Kasting, G.; Beyette, F.; Swaile, D.; Sherman, F.; Joyce, J.; Hagen, J.; Kelley-Loughnane, N.; Naik, R. The microfluidics of the eccrine sweat gland, including

biomarker partitioning, transport, and biosensing implications. *Biomicrofluidics* **2015**, *9* (3), No. 031301.
(73) Haghiashtiani, G.; Qiu, K.; Sanchez, J. D. Z.; Fuenning, Z. J.; Nair, P.; Ahlberg, S. E.; Iaizzo, P. A.; McAlpine, M. C. 3D printed patient-specific aortic root models with internal sensors for minimally invasive applications. *Sci. Adv.* **2020**, *6* (35), No. eabb4641.
(74) Qiu, K.; Zhao, Z.; Haghiashtiani, G.; Guo, S. Z.; He, M.; Su, R.; Zhu, Z.; Bhuiyan, D. B.; Murugan, P.; Meng, F.; et al. 3D Printed Organ Models with Physical Properties of Tissue and Integrated Sensors. *Adv. Mater. Technol.* **2018**, *3* (3), No. 1700235.
(75) Taylor, N. A.; Machado-Moreira, C. A. Regional variations in transepidermal water loss, eccrine sweat gland density, sweat secretion rates and electrolyte composition in resting and exercising humans. *Extreme Physiol. Med.* **2013**, *2* (1), No. 4, DOI: 10.1186/2046-7648-2-4.
(76) Smith, C. J.; Havenith, G. Body mapping of sweating patterns in male athletes in mild exercise-induced hyperthermia. *Eur. J. Appl. Physiol.* **2011**, *111* (7), 1391−1404.
(77) Zhou, Z.; Shu, T.; Sun, Y.; Si, H.; Peng, P.; Su, L.; Zhang, X. Luminescent wearable biosensors based on gold nanocluster networks for "turn-on" detection of Uric acid, glucose and alcohol in sweat. *Biosens. Bioelectron.* **2021**, *192*, No. 113530.
(78) Vaquer, A.; Baron, E.; de la Rica, R. Wearable Analytical Platform with Enzyme-Modulated Dynamic Range for the Simultaneous Colorimetric Detection of Sweat Volume and Sweat Biomarkers. *ACS Sens.* **2021**, *6* (1), 130−136.
(79) Pla-Tolós, J.; Moliner-Martínez, Y.; Molins-Legua, C.; Campíns-Falcó, P. Solid glucose biosensor integrated in a multi-well microplate coupled to a camera-based detector: Application to the multiple analysis of human serum samples. *Sens. Actuators, B* **2018**, *258*, 331−341.

https://doi.org/10.1021/acssensors.4c00528
ACS Sens. 2024, 9, 3212−3223